CHAPTER IV

RESULTS AND DESCUSSIONS

4.1 Properties of Starting Materials

4.1.1 Clay

4.1.1.1 Chemical composition

Chemical composition of original clay (Ratchaburi red clay) was analyzed by X-ray fluorescence (XRF). The analytical result is shown in Table 4.1.

Table 4.1 Chemical composition of clay (Ratchaburi source)

Compositions (wt%)								
SiO_2	Al_2O_3	Fe_2O_3	CaO	MgO	Na_2O	K_2O	TiO_2	L.O.I.
64.25	18.49	4.76	0.63	0.44	<0.01	1.32	0.98	8.18

The main components of the original clay are silica (SiO_2), 64.25 wt%, alumina (Al_2O_3), 18.49 wt%, and iron oxide (Fe_2O_3), 4.76 wt%. There are some amount of calcium oxide (CaO) and potassium oxide (K_2O), which are act as fluxing agent of clay body. Loss on ignition (L.O.I.) value of clay is very high (8.18wt %), because a high quantity of organic matters in clay is burnt out.

As seen in Fig. 4.1, the peaks of kaolinte ($Al_2Si_2O_5(OH)_4$) and muscovite ($KAl_2(Si_3Al)O_{10}(OH)_2$) are observed. The amount of K_2O is 1.32 wt%. Then, the amounts of Al_2O_3 and SiO_2 belonged to muscovite are calculated to be 4.29 wt% and 5.05 wt%, respectively. Therefore, 14.2 wt% of Al_2O_3 belongs to kaolinite. From the molecular notation, the amount of SiO_2 belongs to kaolinite is calculated to be 16.7 wt%. Therefore, 21.75 wt% of SiO_2 belongs to clay. As the result, the amount of quartz is estimated to be 42.5 wt%.

4.1.1.2 Crystal phases

Crystal phases of original clay were characterized by X-ray diffraction (XRD) method. The X-ray diffraction pattern of clay is shown in Fig. 4.1. The main crystal

is quartz, and there are some amounts of kaolinite, muscovite, microcline and hematite crystals. These crystals can be found in general clay.

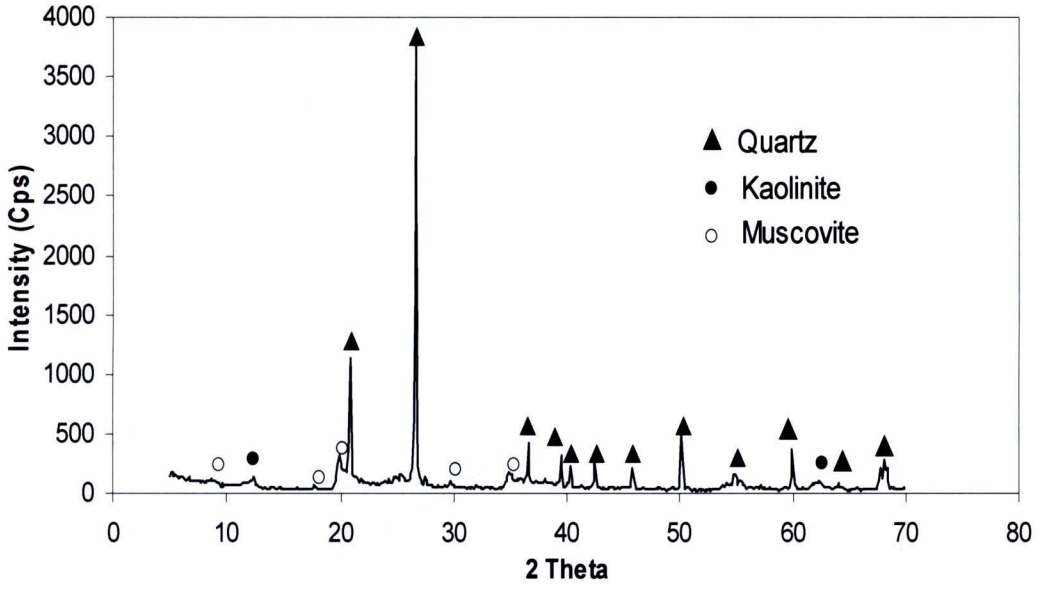

Fig. 4.1 X-ray diffraction pattern of the original clay

4.1.1.3 Microstructure observation and particle size distribution

The particle morphology and particle size distribution of clay are shown in Fig. 4.2 and 4.3, respectively. The particles observed in Fig. 4.2 is quartz because the particle size of clay must be smaller than 2 μm.

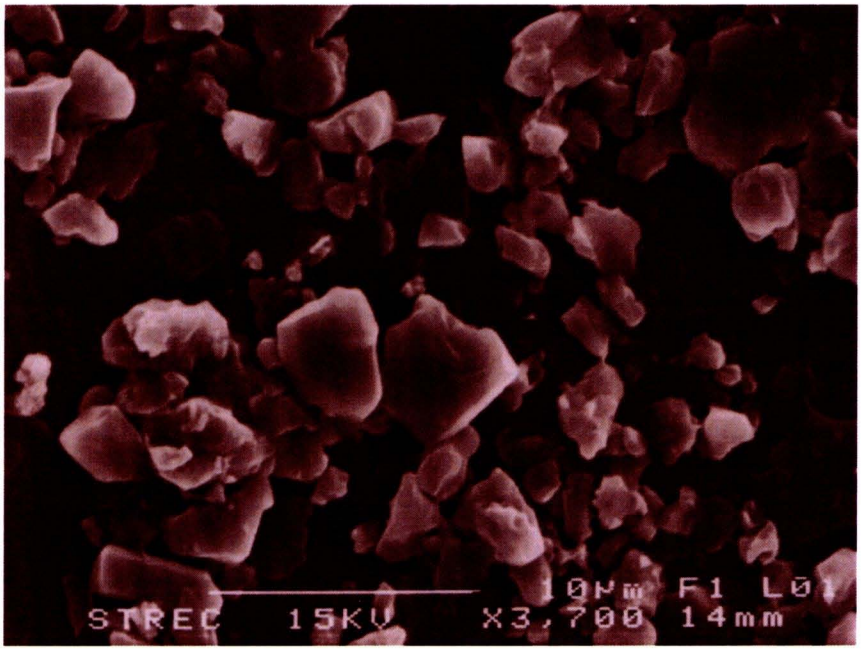

Fig. 4.2 SEM micrograph of original clay

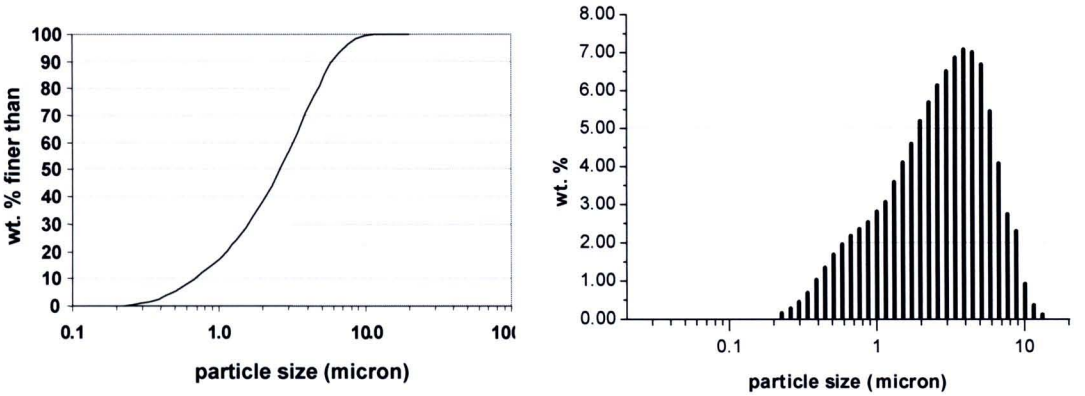

Fig. 4.3 Particle size distribution curve of original clay

The particle size of clay is very small. The range of particle is between 0.2 to 10 μm and the average particle size is only 4 μm. Larger part over 2-3 μm might be quartz and smaller part might be clay.

4.1.1.4 Thermal analysis

Thermal behaviors of clay were analyzed by TG-DTG-DTA unit. TG-DTG-DTA curves of clay are shown in Fig. 4.4.

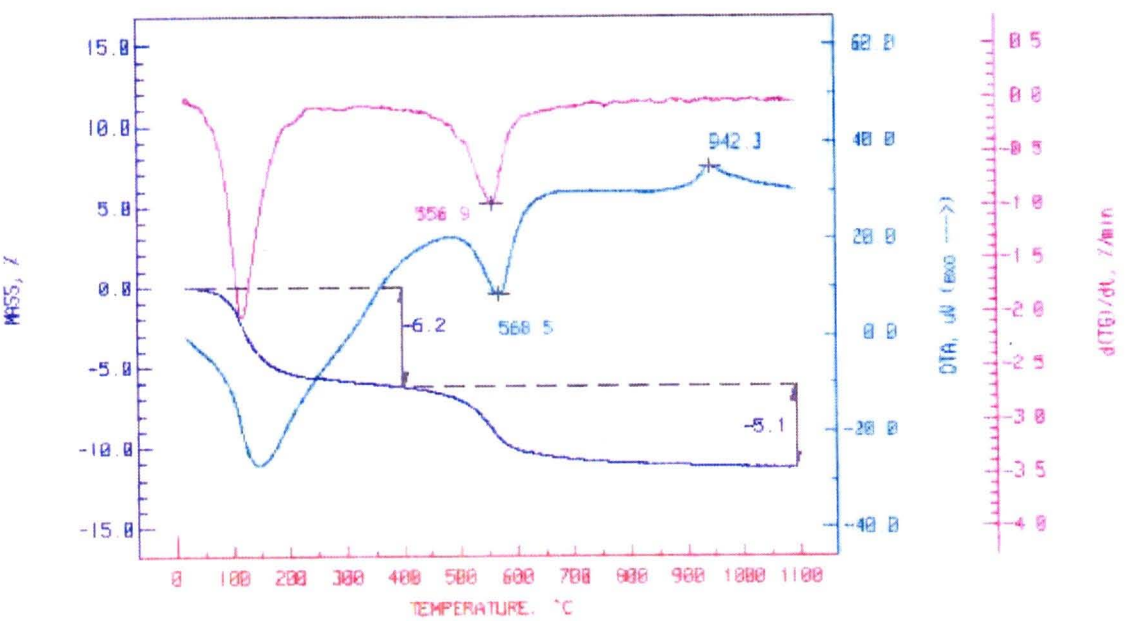

Fig. 4.4 TG-DTG-DTA curves of clay

As indicated in Fig. 4.4, initially, endothermic peak occurs at about 100-200 °C, caused by the removal of absorbed water of clay. At about 500-600 °C the main endothermic peak commences, the tip of the peak being at about 569 °C, corresponding to the decomposition of clays, and the elimination of the hydroxyl groups as water. A further peak, which is exothermic, occurs at about 950 °C. It is associated with the recrystallization process. The mineral which is decomposed is kaolinite and the new crystal phase from the recrystallization process might be silicon spinel. The decomposition and recrystallization reactions of kaolinite are shown in reaction (1) and (3) *(10)*

$$Al_2Si_2O_5(OH)_4 \xrightarrow{450°C} Al_2Si_2O_7 + 2H_2O \quad \text{----------(1)}$$

Kaolinite Metakaolin

$$2(Al_2O_3.2SiO_2) \xrightarrow{925°C} 2Al_2O_3.3SiO_2 + SiO_2 \quad \text{----------(2)}$$

Metakaolin Silicon spinel

$$2Al_2O_3.3SiO_2 \xrightarrow{1100°C} 2(Al_2O_3.SiO_2) + SiO_2 \quad \text{----------(3)}$$

Silicon spinel pseudo-mullite

Mass losses are observed from TG-DTG curve, which correspond to the removal of absorbed water and decomposition of combined water of clay. Total mass loss of clay from TG curve is about 11.3 wt%. This amount is a little larger than the value of L.O.I. (8.18wt%) by chemical analysis.

4.1.2 Rice husk ash (RHA)

4.1.2.1 Chemical composition

Chemical composition of rice husk ash (RHA) was analyzed by X-ray fluorescence (XRF). The analytical result is shown in Table 4.2.

Table 4.2 Chemical compositions of RHA

Compositions (wt%)								
SiO_2	Al_2O_3	Fe_2O_3	CaO	MgO	Na_2O	K_2O	TiO_2	L.O.I.
89.65	<0.01	0.19	0.87	0.40	<0.01	2.26	<0.01	5.05

As shown in Table 4.2, the main element in RHA is silicon (89.64 wt% as SiO_2). Other minor components are potassium (2.26 wt% as K_2O), calcium, iron and magnesium oxides. Loss on ignition at 1100 °C is 5.05 wt%, caused by the decomposition of unburned carbon in RHA.

4.1.2.2 Crystal phase

Phase compositions of RHA were characterized by X-ray diffraction (XRD). The X-ray diffraction pattern of RHA is shown in Fig. 4.5. The main crystal phase is cristobalite. Generally, cristobalite phase in RHA can be formed at firing temperature above 700 °C.*(7)* D.M. Ibrahim et al.*(22)* reported that the crystallization become conspicuous in the RHA fired at 900°C. The X-ray pattern of low form cristobalite was obtained at 1000°C. The peaks were broadened but sharpened with increase of firing temperature. Since RHA in this experiment was obtained from by-product of rice mill industry, it was burnt at rather high temperature (>700 °C) to get high energy for electrical power. Therefore, the main crystal phase of this RHA is cristobalite.

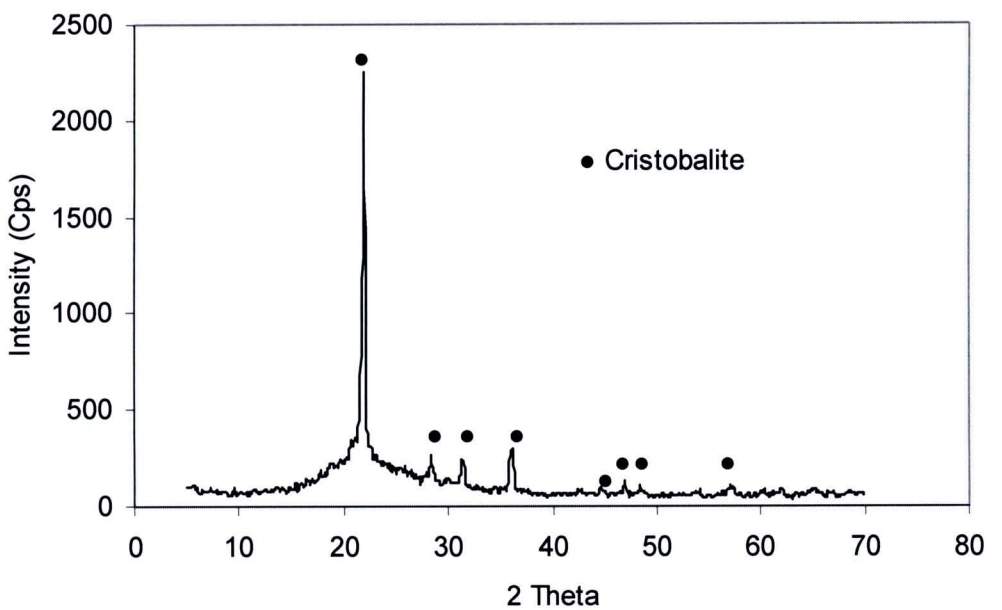

Fig. 4.5 X-ray diffraction pattern of rice husk ash

4.1.2.3 Microstructure observation

SEM micrographs of rice husk ash with the particle size under 50 and 100 mesh are shown in Fig. 4.6 and 4.7, respectively. As indicated in Fig. 4.8, the surface of RHA shows the porous surface.

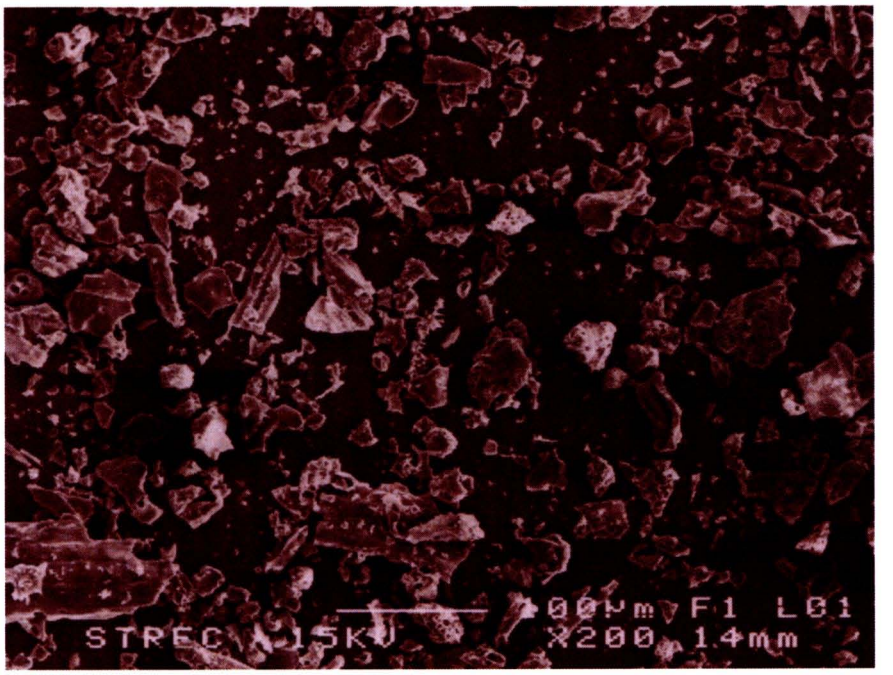

Fig. 4.6 SEM micrograph of rice husk ash, particle size under 50 mesh

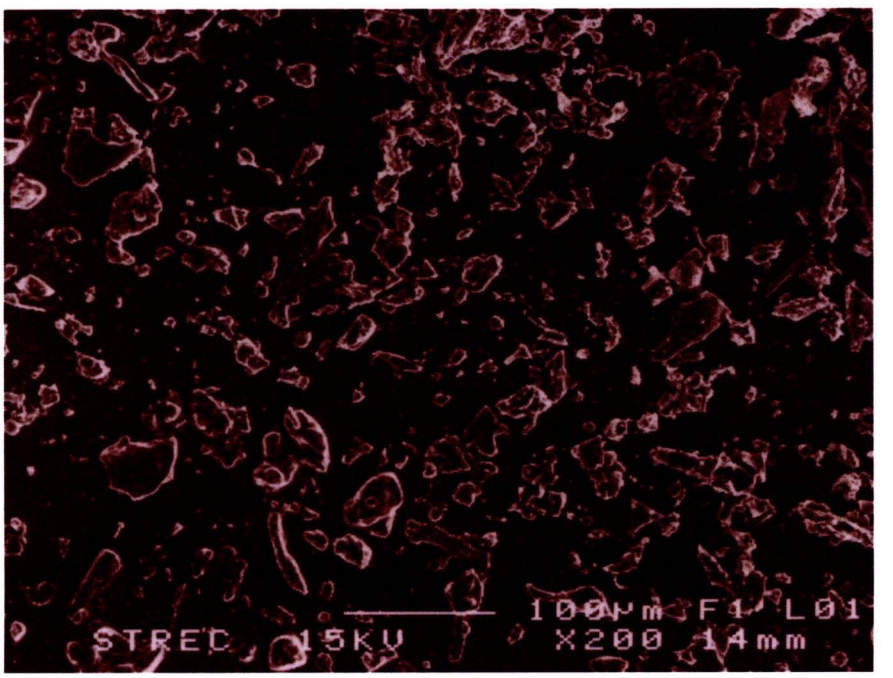

Fig. 4.7 SEM micrograph of rice husk ash, particle size under 100 mesh

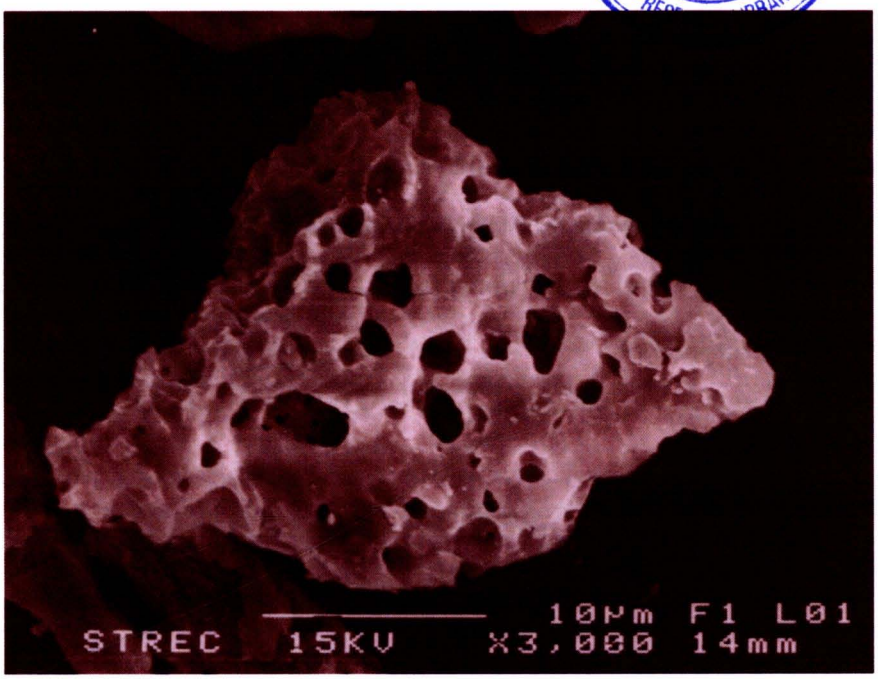

Fig. 4.8 SEM micrograph of the surface of rice husk ash particle size

4.1.2.4 Thermal analysis

Thermal behaviors of RHA carried out by TG-DTG-DTA unit. TG-DTG-DTA curves of RHA are shown in Fig. 4.9.

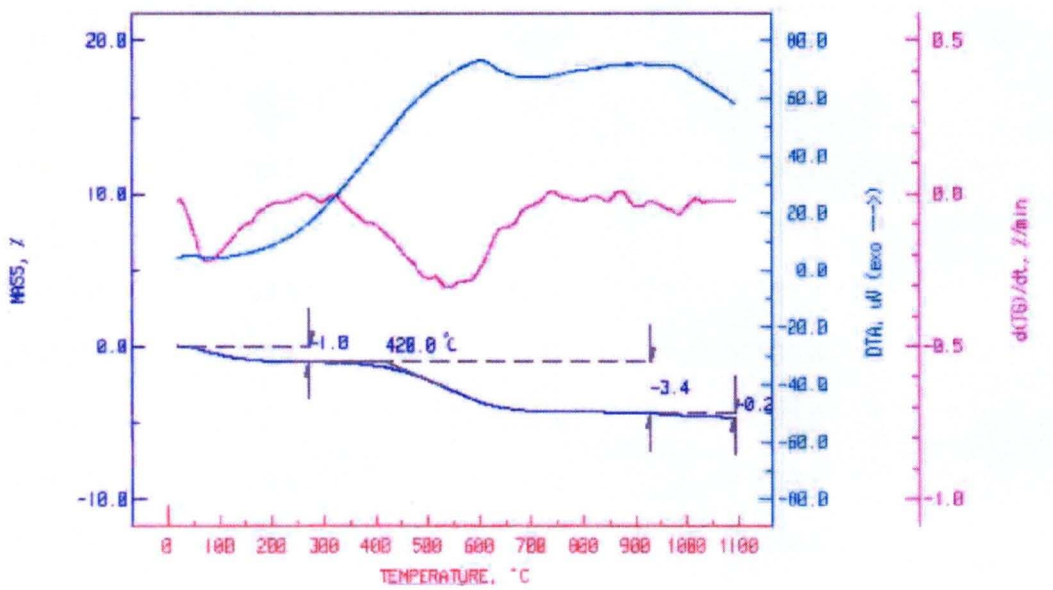

Fig. 4.9 TG-DTG-DTA curves of rice husk ash

As indicated in Fig. 4.9, initially, at about 100 °C, small amount of mass loss occurs. It is thought to be caused by the removal of adsorbed water in RHA. Further DTG peak occurs at about 300-600 °C, the tip of the peak being at about 550 °C, caused by the burning of carbonaceous matters residue in RHA. The total mass loss of RHA is about 4.4 wt%. The DTA shows a prominent exotherm at about 600 ° C which is attributed to the burning of remained carbon in RHA. J. James and M. Subba Rao *(23)* reported that the thermal decomposition behaviour of cellulose and lignin had been investigated in relation to the pyrolysis of wood. Cellulose and lignin were reported to decompose in the temperature ranges 600-650 °C and 500-773 °C, respectively.

4.2 Properties of Mixed Clay and Sintered Specimens

4.2.1 Plasticity of clay and mixed clay

Plasticity of clay and mixed clay with various content of RHA was determined by Atterberg's limit test. The results are shown in Table 4.3 and the total experimental data are shown in Appendix A.

Table 4.3 Plastic properties of clay and mixed clay

Formula	Liquid limit (L.L.) (%)	Plastic limit (P.L.) (%)	Plasticity index (Ip) (%)
NC	65.4	20.8	44.6
NF	55.2	18.9	36.3
NS50	56.0	19.2	36.8
NS100	53.3	18.0	35.3
3RHA50	54.1	16.7	37.4
3RHA100	52.4	17.0	35.4
6RHA50	52.4	16.5	35.9
6RHA100	50.4	16.6	33.8
9RHA50	51.4	17.0	34.4
9RHA100	49.5	17.6	31.9

As shown in Table 4.3, liquid limit, plastic limit and plasticity index decrease when RHA content increases. In addition, the plasticity indices of mixed clay with smaller particle size RHA are smaller than that of the larger particle size one. From this data, it can be concluded that RHA can reduce the plasticity of the clay body.

4.2.2 Drying rate and drying shrinkage

Drying rate and drying shrinkage graphs at room temperature of mixed clay with different contents of RHA are shown in Fig. 4.10 and 4.11, respectively.

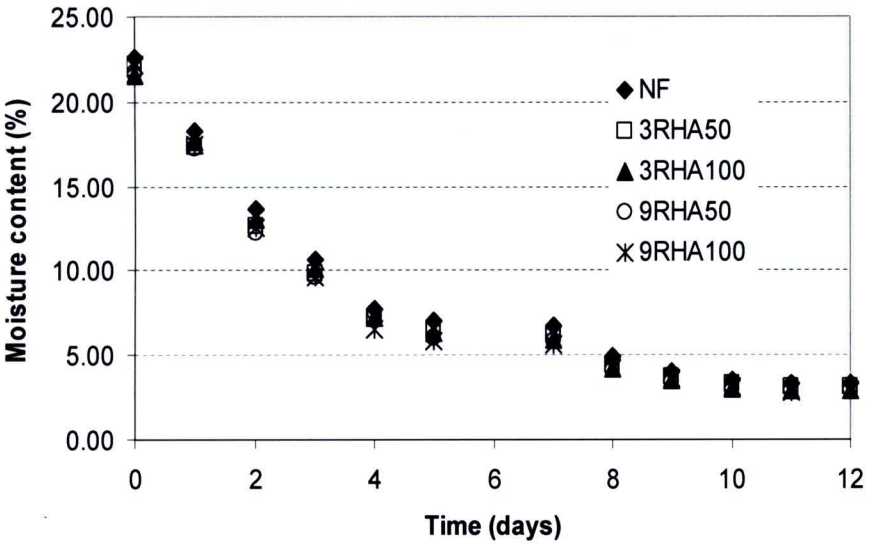

Fig. 4.10 Drying rate curves at room temperature of mixed clay body

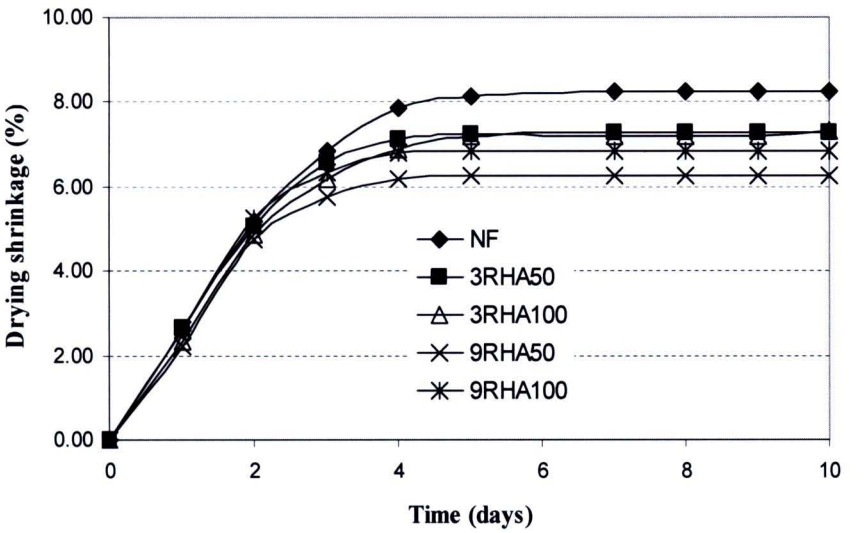

Fig. 4.11 Drying shrinkage curves at room temperature of mixed clay body

As indicated in Fig. 4.10, drying rate of each composition does not show a big difference even though the 9wt% of RHA was added. However, comparison of the normal formula (NF) with mixed clay body of 9 wt% of RHA (-100#, 9RHA100), the drying rate of the normal formula is slower than 9RHA100 (moisture content of normal formula is higher). This result corresponds to the one fact of the fundamentals of clay body drying that nonplastic materials can increase drying rate of clay body.*(12)* The amount of moisture did not change during day 4 to 6, because at that time the weather was humid.

In case of drying shrinkage, as shown in Fig. 4.11, Initially, drying shrinkage curves of all formulas are linear from the starting time to 3 days, but in the later stage the curves become exponential. Then, drying shrinkage becomes constant after 4 days. It means that the body does not shrink after 4 days even the moisture decreases. Drying shrinkage values at room temperature are decreased when the RHA content in mixed clay bodies increases. In addition, shrinkage after drying at 110 °C also decreases when RHA is added, as shown in Fig. 4.12. Moreover, the larger particle size of RHA shows less drying shrinkage than smaller particle size at 9 wt% RHA.

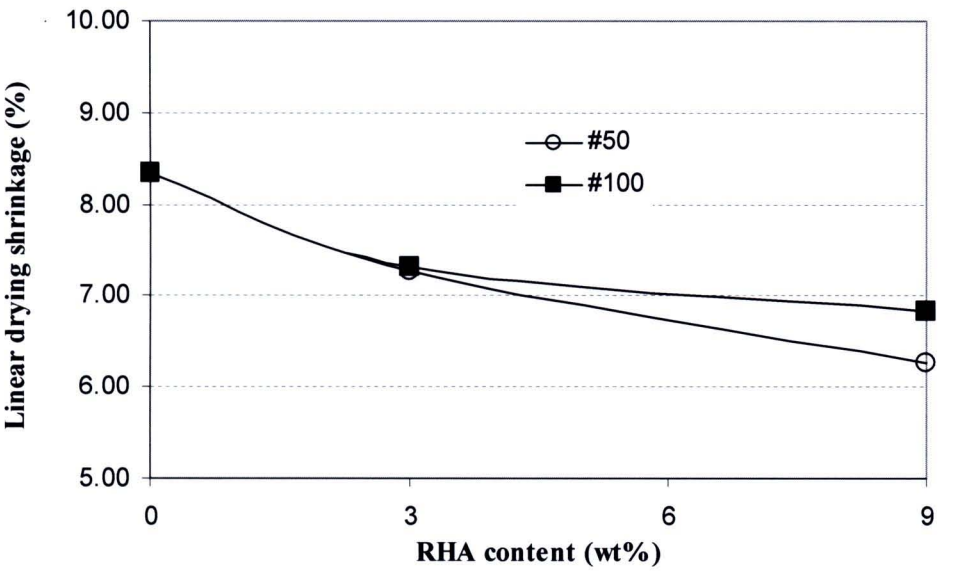

Fig. 4.12 Effect of quantity and particle size of RHA on drying shrinkage of mixed clay bodies, dried at 110 °C

4.2.3 Firing shrinkage

The linear firing shrinkage of all formulas at the firing temperature of 900, 950, 1000, 1050 and 1100 °C are shown in Fig.4.13. The graph shows that the linear firing shrinkage is reduced with increasing quantity of RHA, especially when firing temperature is over 950 °C. Fig. 4.14 shows the linear fired shrinkage of all formulas fired at 950 °C. The total experimental data is shown in Appendix B.

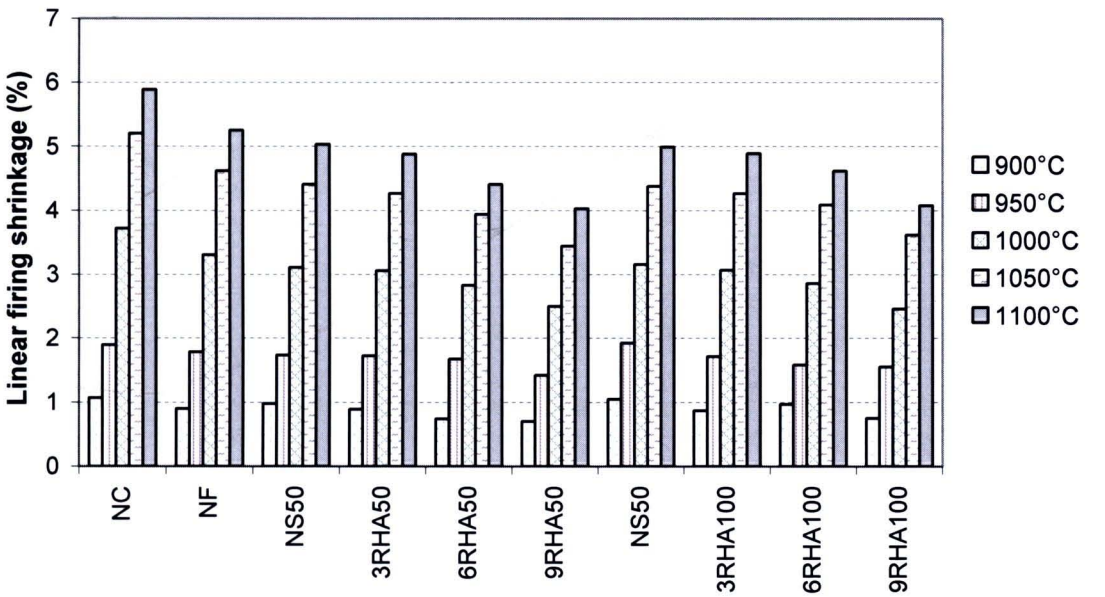

Fig 4.13 Linear firing shrinkage of fired mixed clay bodies at various temperatures

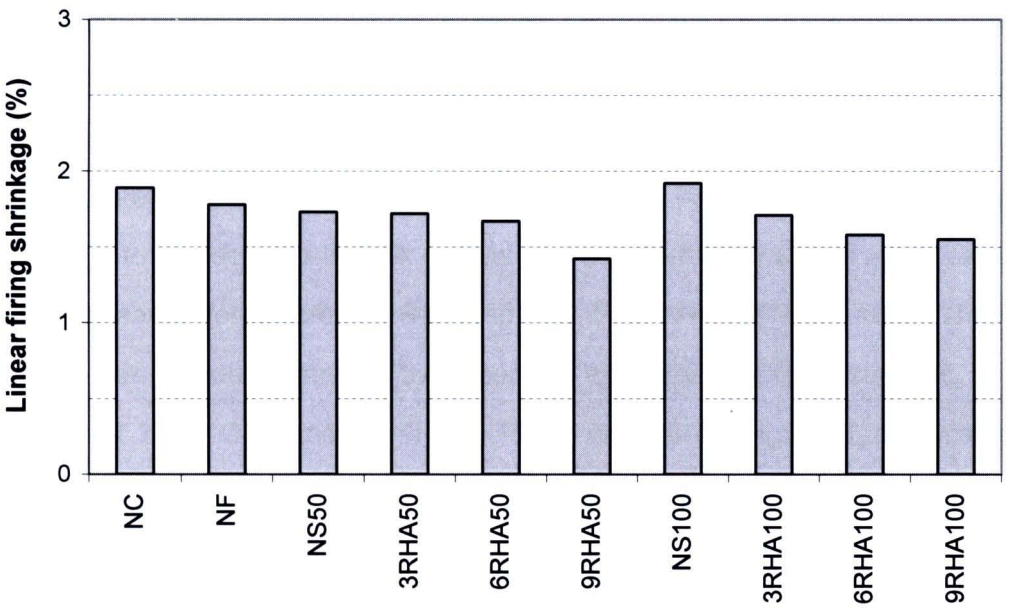

Fig 4.14 Linear firing shrinkage of fired mixed clay bodies at 950 °C

Fig. 4.15 shows the linear firing shrinkage as a function of firing temperature. The shrinkage decreased with the amount of adding RHA.

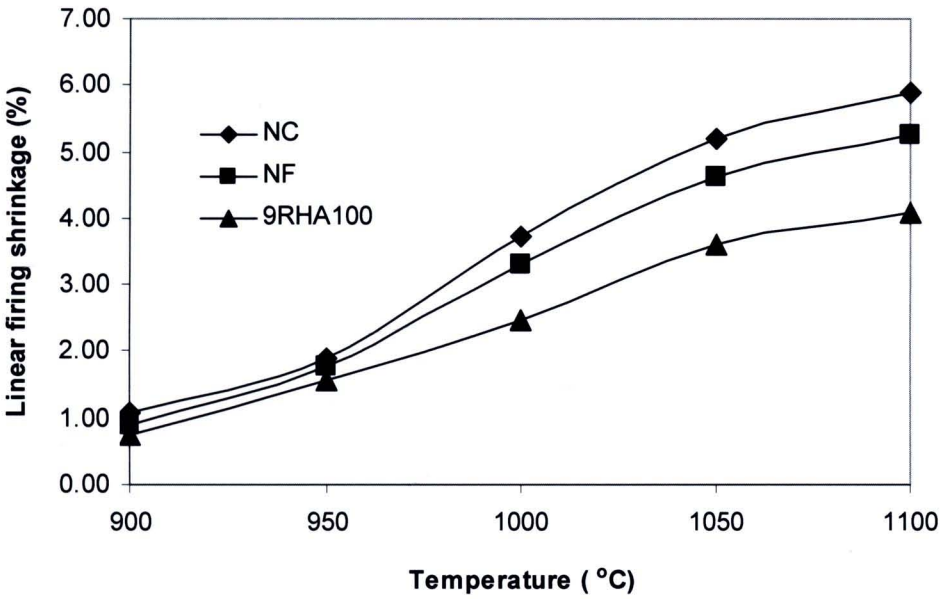

Fig 4.15 Linear firing shrinkage of fired natural clay (NC), normal formula (NF) and 9RHA100 at various temperatures.

4.2.4 Bulk density and water absorption

The bulk density of all formulas at the firing temperature of 900, 950, 1000, 1050 and 1100 °C are shown in Fig.4.16.The graphs show that bulk density is reduced with the increasing quantity of RHA. Fig. 4.17 shows the bulk densities of all formulas firing at 950 °C. Fig. 4.19 shows that the bulk density increases with increasing the firing temperatures and decreases with increasing the amount of RHA. The reduction of bulk density is surely caused by the increasing of porosity in the body. The increment of porosity due to the increase in RHA content might come from the burn out of carbon in RHA, which leaves some pores behind. Also, SiO_2 from RHA might disturb the shrinkage of clay. It can be demonstrated by observing the cross sectional surfaces of fired specimens at 1000 °C as shown in Fig. 4.18. As indicated in Fig. 4.18, the small black spots might be the remained porosity from the burn out of carbon. All of experimental data are shown in Appendix C.

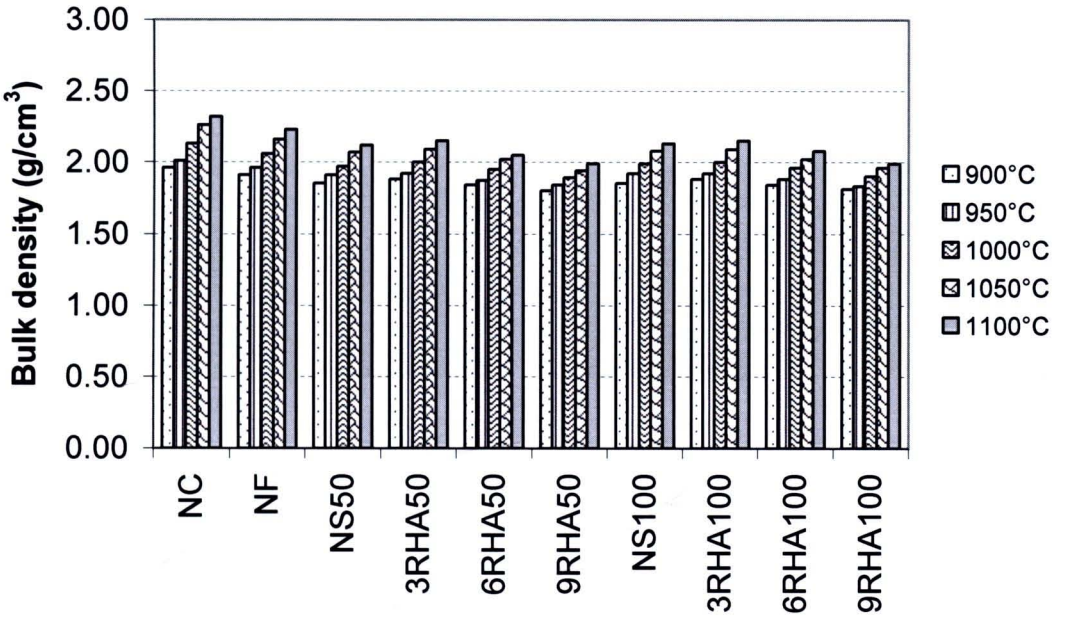

Fig 4.16 Bulk densities of fired mixed clay bodies at various temperatures

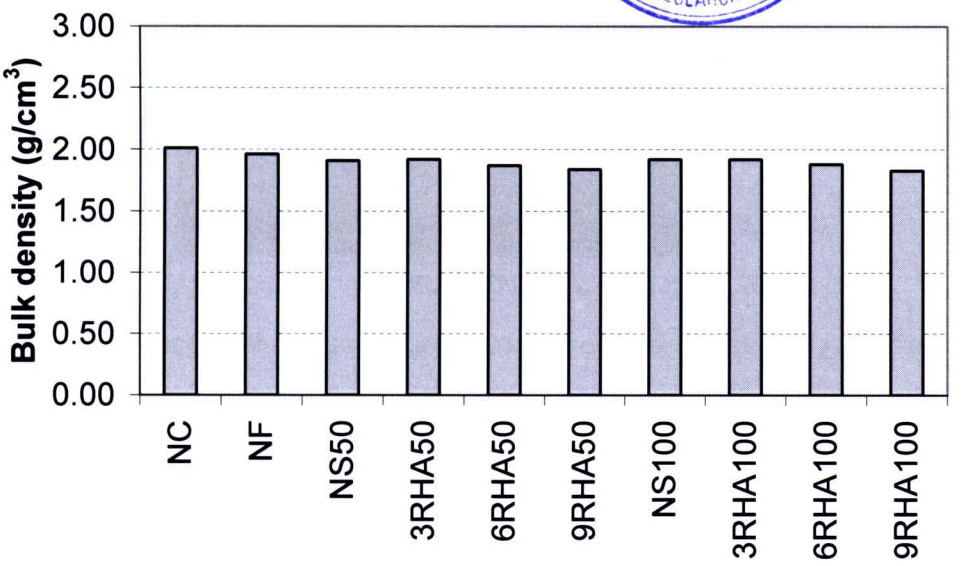

Fig 4.17 Bulk densities of fired mixed clay bodies at 950 °C

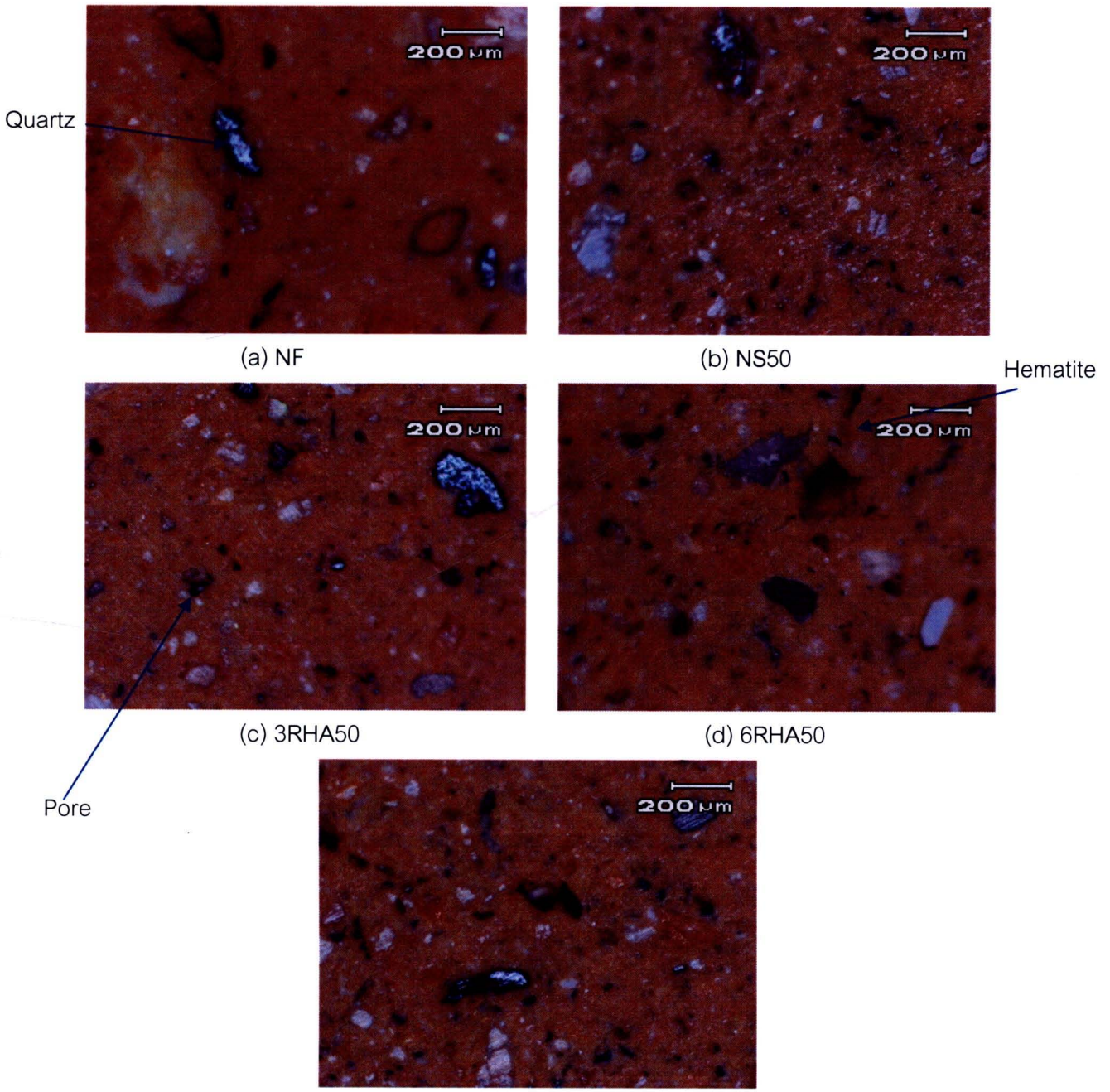

Fig. 4.18 The images of cross sectional surfaces of fired mixed bodies at 1000 °C by optical microscope

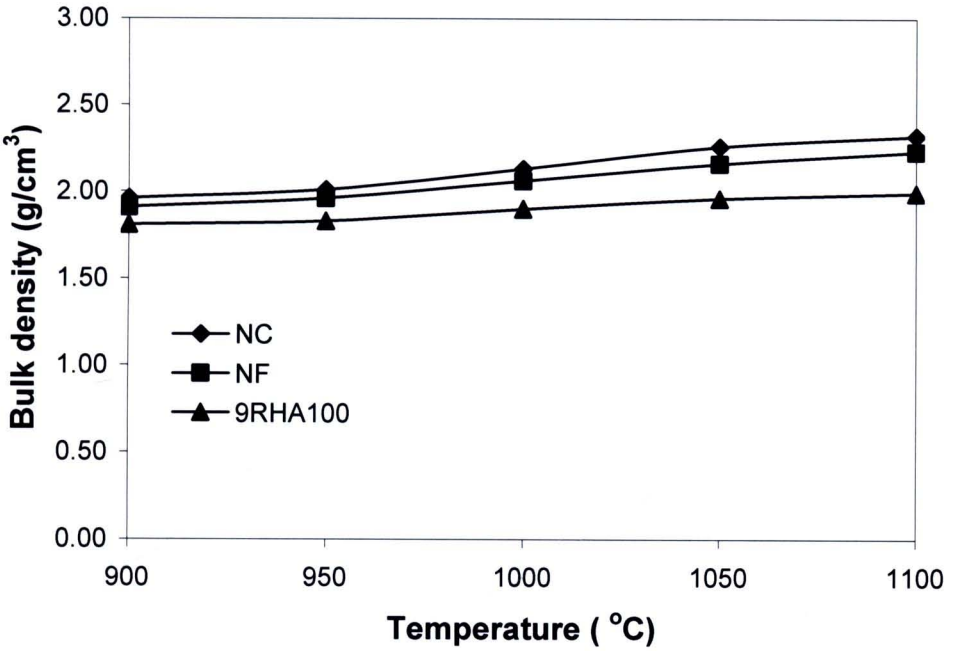

Fig 4.19 Bulk density of fired natural clay (NC), normal formula (NF) and 9RHA100 at various temperatures

The water absorption of all formulas at the firing temperature of 900, 950, 1000, 1050 and 1100 °C are shown in Fig.4.20. The graph shows that the water absorption increased with the increasing quantity of RHA. Fig.4.21 shows the water absorption of all formulas firing at 950 °C. Fig 4.22 shows that the water absorption decreases with increasing the firing temperature but increases with increasing the amount of RHA.

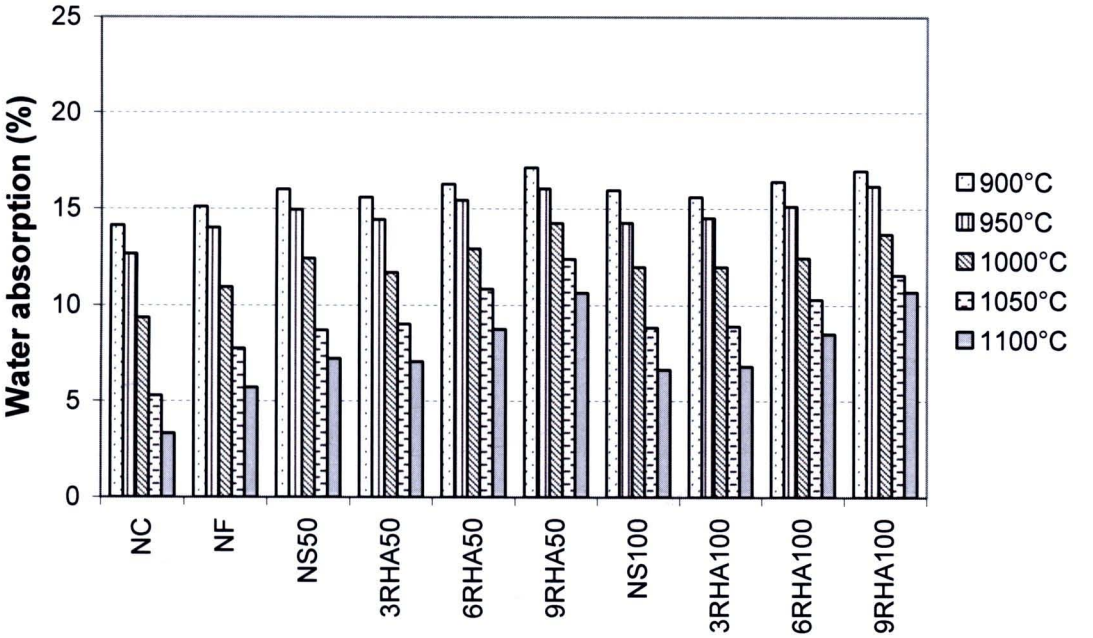

Fig 4.20 Water absorption of fired mixed clay bodies at various temperatures

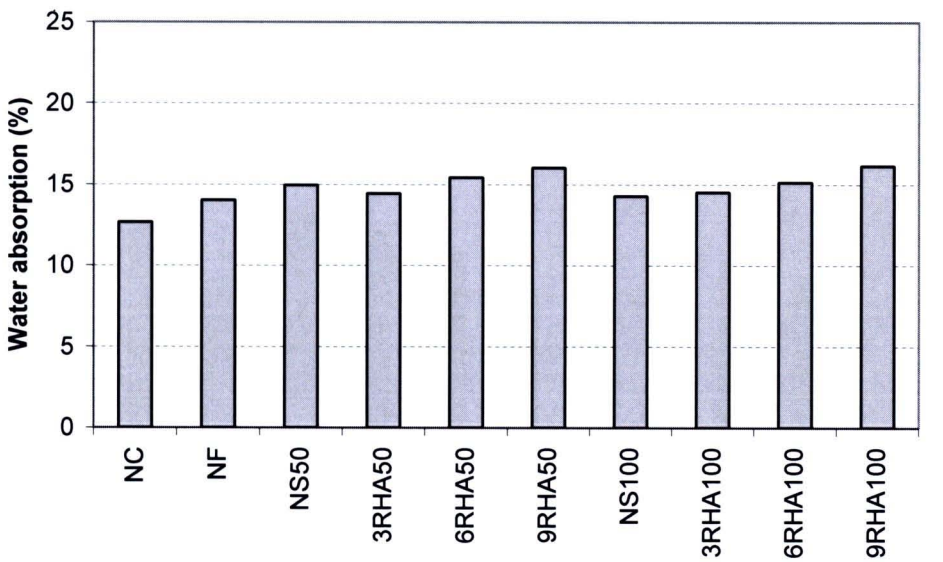

Fig 4.21 Water absorption of fired mixed clay bodies at 950 °C

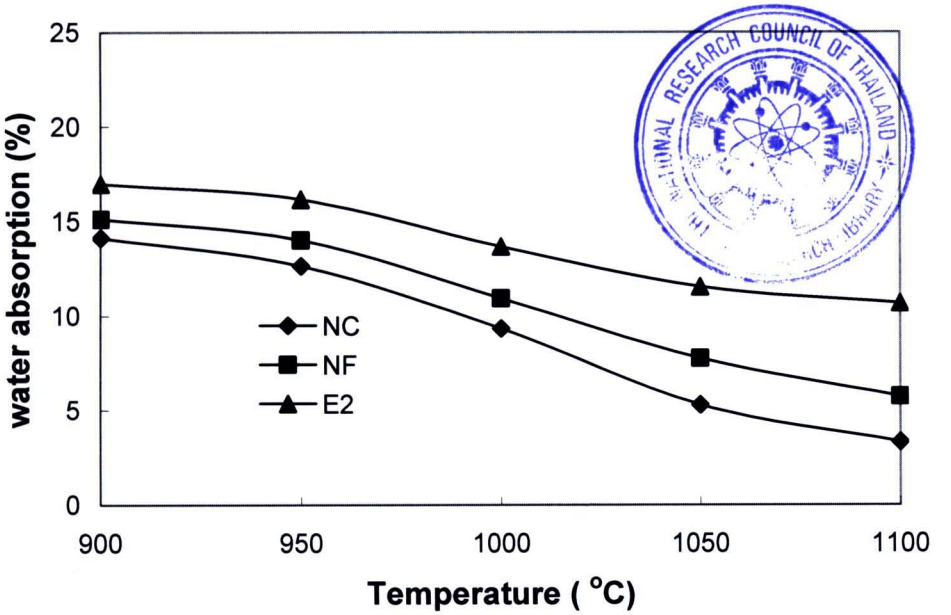

Fig 4.22 Water absorption of fired natural clay (NC), normal formula (NF) and 9RHA100 at various temperatures.

4.2.5 Modulus of rupture of green body and fired specimens

The modulus of rupture of green specimens is shown in Fig. 4.23. The total experimental data is shown in Appendix D.

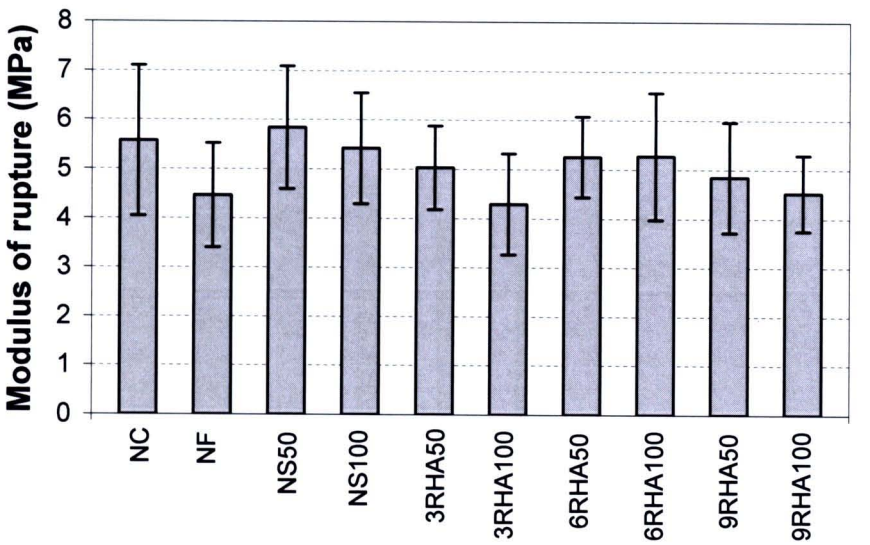

Fig 4.23 Modulus of rupture of green bodies

The moduli of rupture of all formulas at the firing temperature of 900, 950, 1000, 1050 and 1100 °C are shown in Fig.4.24 and the experimental data are shown in Appendix E. Comparing to the normal formula (NF), the modulus of rupture does not change with the addition of only 3 wt% RHA (3RHA50, 3RHA100). But the modulus of rupture decreases when the quantity of RHA in the mixed clay bodies increases to 6 wt% (6RHA50, 6RHA100) or 9 wt% (9RHA50, 9RHA100). Fig. 4.25 shows the moduli of rupture of all formulas firing at 950 °C.

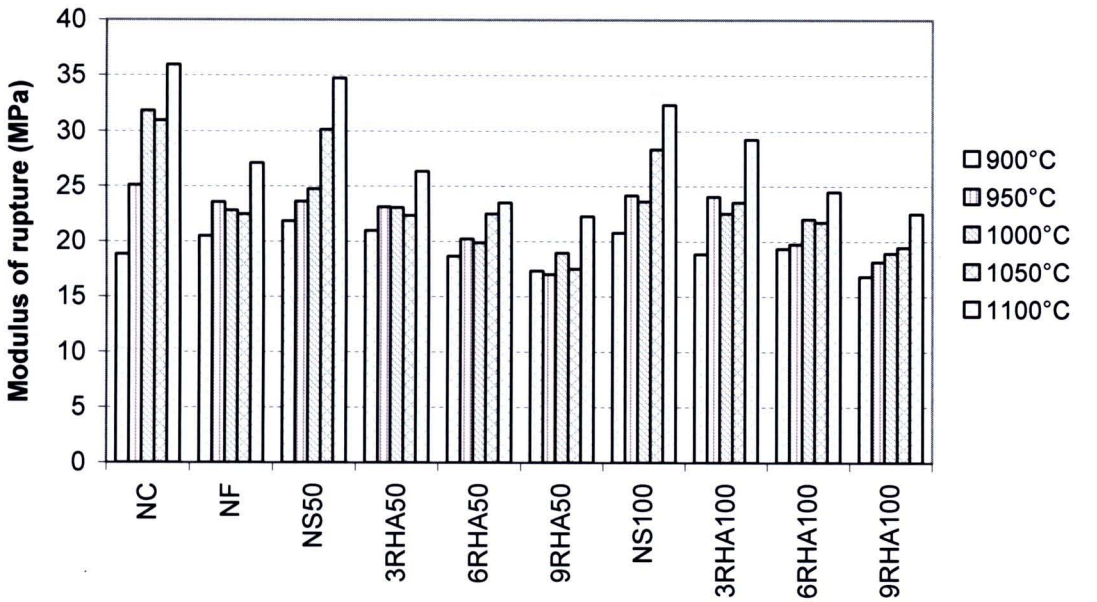

Fig 4.24 Modulus of rupture of fired mixed clay bodies at various temperatures

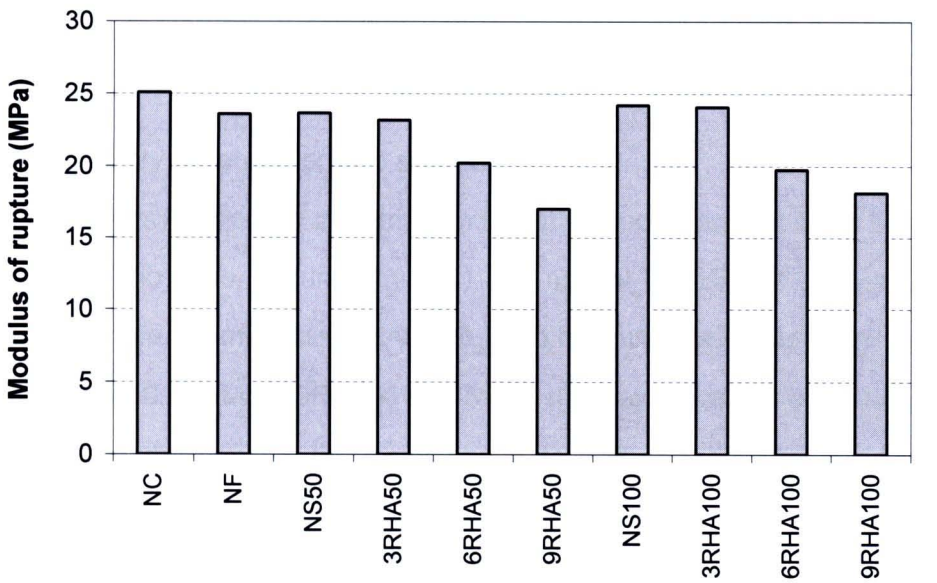

Fig 4.25 Modulus of rupture of fired mixed clay bodies at 950 °C

In the formula NS50 and NS100 which are the compositions that silica sand was completely replaced by RHA, the modulus of rupture significantly increases especially when the firing temperature is over 950 °C as shown in Fig. 4.26. Moreover, at the firing temperature above 950°C, the modulus of rupture of NS50 and NS100 are higher than NF. It might be attributed to stronger pre-stress caused by the difference in coefficient of thermal expansion between cristobalite phase and other components in the fired body. *(24)*

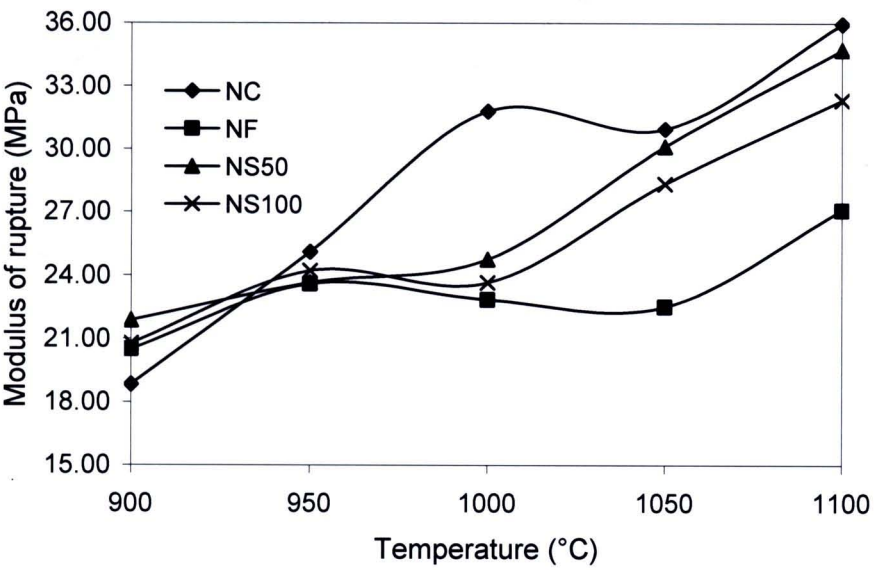

Fig 4.26 Modulus of rupture of fired natural clay (NC), normal formula (NF), NS50 and NS100 at various temperatures

4.2.6 Crystal phase of fired specimens

The X-ray diffraction patterns of mixed clay bodies fired at 1000 °C are shown in Fig. 4.27. In the case of pure clay (PC) and normal formula (NF), the major phase is quartz and there are microcline ($KAl_2Si_3O_8$) and hematite (Fe_2O_3) as minor phases. In the case of 3RHA50, 6RHA50, 9RHA50 and NS50, the major phase is also quartz (SiO_2), but cristobalite is observed as the minor phase as well as microcline and hematite. This cristobalite might come from the RHA, because the RHA consists of cristobalite as a major phase (see Fig. 4.5). It can be confirmed by considering the formulas of 3RHA50, 6RHA50 and 9RHA50 that the intensity of cristobalite phase increases when the RHA content is increased from 3wt% to 9wt%.

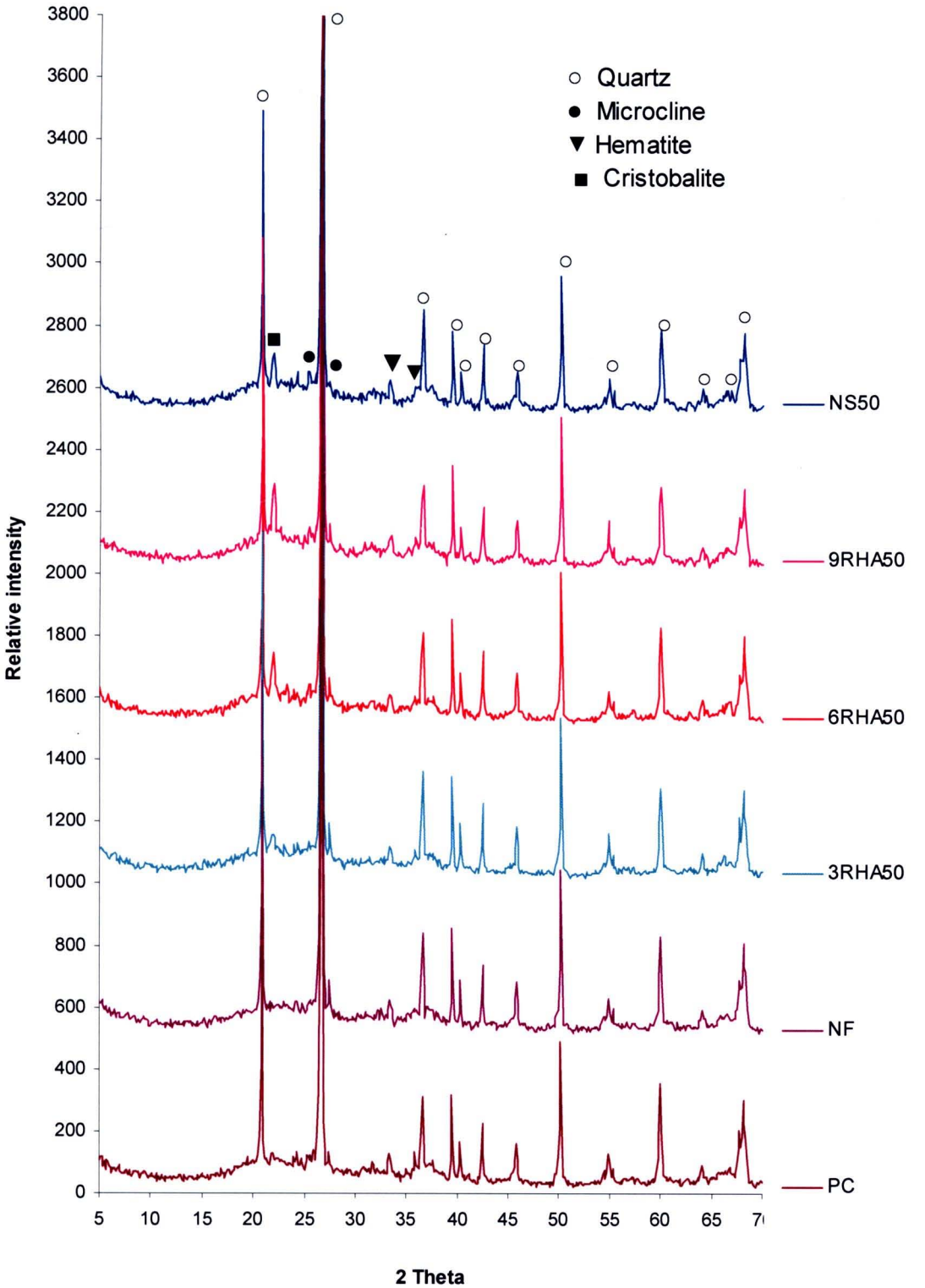

Fig 4.27 X-ray diffraction patterns of mixed clay bodies firing at 1000 °C